Broad band nonreciprocal directional dichroism in Ni_3TeO_6

M. O. Yokosuk,[1] Heung-Sik Kim,[2,3] K. D. Hughey,[1] Jaewook Kim,[2,4] A. V. Stier,[5] K. R. O'Neal,[6] Junjie Yang,[7] S. Crooker,[5] K. Haule,[2] Sang-Wook Cheong,[2,8,4] David Vanderbilt,[2] and J. L. Musfeldt[1,9,*]

[1]*Department of Chemistry, University of Tennessee, Knoxville, Tennessee 37996, USA*
[2]*Department of Physics and Astronomy, Rutgers University, Piscataway, New Jersey 08854, USA*
[3]*Department of Physics, Kangwon National University, Chuncheon 24341, Korea*
[4]*Rutgers Center for Emergent Materials, Rutgers University, Piscataway, New Jersey 08854, USA*
[5]*National High Magnetic Field Laboratory, Los Alamos, New Mexico 87545, USA*
[6]*Department of Chemistry, University of Tennessee, Knoxville, Tennessee 37996 USA*
[7]*Department of Physics and The Science of Advanced Materials Program, Central Michigan University, Mount Pleasant, Michigan 48858, USA*
[8]*Laboratory for Pohang Emergent Materials and Max Planck POSTECH Center for Complex Phase Materials, Pohang University of Science and Technology, Pohang 790-784, Korea*
[9]*Department of Physics and Astronomy, University of Tennessee, Knoxville, Tennessee 37996, USA*

(Dated: June 17, 2019)

Nonreciprocal directional dichroism is an unusual light-matter interaction that gives rise to diode-like behavior in low symmetry materials. The chiral varieties are particularly scarce due to the requirements for strong spin-orbit coupling, broken time reversal symmetry, and a chiral axis. We bring together magneto-optical spectroscopy and first principles calculations to reveal high energy, broad band nonreciprocal directional dichroism in Ni_3TeO_6 with special focus on behavior in the metamagnetic phase above 52 T. In addition to demonstrating this effect in the magnetochiral configuration, we explore the transverse magnetochiral orientation in which applied field and light propagation are orthogonal to the chiral axis and by so doing, uncover an additional configuration with nonreciprocal directional dichroism in the visible part of the spectrum. Using first principles methods, we analyze how the Ni^{2+} d-to-d on-site excitations develop magnetoelectric character and present a microscopic model that unlocks the door to theory-driven discovery of chiral magnets with nonreciprocal directional dichroism.

Strong spin-orbit coupling and broken symmetries give rise to many novel properties in materials. One of the more peculiar is nonreciprocal directional dichroism or "one-way transparency" [1, 2]. A nonreciprocal effect occurs when the motion of an object in one direction is different from that in the opposite direction [3]. Electrical transport in chiral WS_2 nanotubes [4] and layered $CrNb_3S_6$ [5], spin wave nonreciprocity in magnetic TaPy bilayers [6] and antiferromagnetic $Ba_3NbFe_3Si_2O_{14}$ [7], and propagation of excitations along skyrmion strings in chiral Cu_2OSeO_3 [8] are proof-of-concept examples. Spectroscopically, the effect occurs in the vicinity of a magnetoelectric excitation and arises from how absorption depends on the light propagation direction [1, 3, 9]. Thus a given sample may be highly transmitting when measured with light propagating in the $+k$ direction, but strongly absorbing for light in the $-k$ direction.

There are stringent symmetry requirements in order for a nonreciprocal effect to occur. For a given propagation direction $\hat{k}$, all symmetries that would reverse k to $-k$ must be broken, including inversion, mirrors or C_2 rotations about a plane or axis perpendicular to $\hat{k}$, and time reversal [3, 9]. As one might anticipate, this is relatively rare. There are several different measurement configurations that can be used to take advantage of various types of symmetry breaking [3]. Toroidal dichroism is the most well studied case [10–12]. It occurs when light propagation is along the toroidal moment $\boldsymbol{T}$, ($k \parallel \boldsymbol{T} = \boldsymbol{P} \times \boldsymbol{M}$, where $\boldsymbol{P}$ and $\boldsymbol{M}$ are the electric polarization and magnetic moment of the material, respectively). A second, less common mechanism takes place in chiral magnets [13–21]. Here, light can be directed along the chiral axis and the external field direction. This nonreciprocal effect is called magnetochiral dichroism. We also point out that while it is often anticipated that linearly or circularly polarized light must be used to induce a nonreciprocal response, unpolarized light can also reveal the effect [22].

Because nonreciprocal directional dichroism depends upon both the electric and magnetic dipole matrix elements [1], magnetoelectric multiferroics - with their low crystallographic and magnetic symmetries - are promising platforms in which to search for these effects. Most materials identified so far have been studied in the terahertz region in order to reveal nonreciprocity in the vicinity of the electromagnon. Examples include $BiFeO_3$ [23, 24], $CaBaCo_4O_7$ [11], $FeZnMo_3O_8$ [22], and $Ba_2CoGe_2O_7$ [10, 13]. An electromagnon has natural magnetoelectric character, and the energy scale of the

* musfeldt@utk.edu

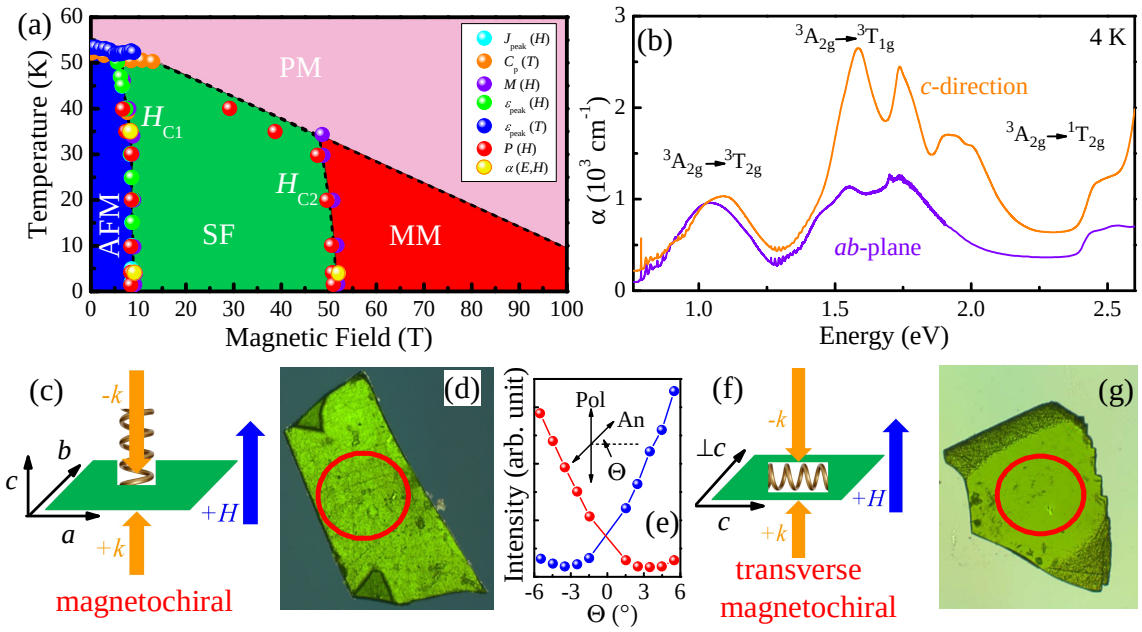

FIG. 1. **Phase diagram, optical properties, and measurement geometries of Ni_3TeO_6.** (a) Comprehensive H - T phase diagram [25–27]. (b) Optical absorption spectrum of Ni_3TeO_6. The on-site Ni d-to-d excitations are labeled [27]. (c) Schematic representation of magnetochiral dichroism. This measurement orientation requires a chiral axis in the material as well as light ($\pm k$) and magnetic field $\pm H$ aligned along the chiral direction in the Faraday geometry. The nonreciprocal effect will depend upon light propagation and field direction. The symmetry considerations are fully discussed in the Supplementary Information. (d) Image of the ab-plane sample under crossed linear polarizer and analyzer. The red circle indicates the position of the light spot, which is within a single chiral domain. (e) Optical rotation measurement using crossed polarizer and analyzer. The angle Θ corresponds to the angle between the analyzer and normal from the polarizer. The red symbols correspond to the lighter green portion of the crystal, and the blue symbols correspond to the darker green portion in the corners. (f) The nonreciprocal effect also occurs in the transverse magnetochiral orientation. Here, we maintain the Faraday geometry (with $\pm k$ and $\pm H$) but the chiral (c) axis is in the plane of the polished crystal. Again, the symmetry considerations are discussed in the Supplementary Information. (g) Image of the polished crystal in which the c-axis is exposed under crossed linear polarizer and analyzer. The red circle indicates the measurement region which is within a single chiral domain.

light and that of the spins is similar. There are also examples of broad band nonreciprocal directional dichroism at higher energies - for instance in $GaFeO_3$ [28] and CuB_2O_4 [14, 15, 29–31]. In many of the aforementioned cases, the authors reversed the direction of the external magnetic field rather than the light propagation direction. This approach has clear experimental advantages and is valid for materials with a switchable magnetic moment. Whether the effect is actually symmetric (or not) is highly under-explored.

Ni_3TeO_6 is a superb system with which to test these ideas of nonreciprocity. The material sports one of the largest magnetoelectric coupling constants to date [25, 26]. The crystal structure is corundum-like with an $R3$ space group [32]. Each Ni and Te ion is surrounded by six oxygen centers - all of which are inequivalent [32]. In addition to a Ni1, Ni2, Ni3, Te alignment along c, the $R3$ space group supports a c-directed chiral axis [33]. The magnetic field - temperature (H - T) phase diagram in Fig. 1(a) summarizes the important energy scales [25, 26]. Below T_N = 53 K, the Ni spins align to form a collinear antiferromanget (AFM). Polarization grows substantially below T_N. Under magnetic field ($H \parallel c$), there is a 9 T spin flop (SF) and a 52 T transition to the metamagnetic (MM) phase. Polarization can be controlled across both of these magnetically-driven transitions [25, 26]. The optical absorption of Ni_3TeO_6 is summarized in Fig. 1(b). These features are assigned as Ni d-to-d on-site excitations, and the anisotropy is a consequence of the crystal structure [27]. In a material like Ni_3TeO_6, the direction of the chiral axis and the pitch of the chiral rotation [33] impacts the magneto-optical response. There are two orientations of interest. In panel (c), the chiral axis is out of the ab-plane, whereas in panel (f), the chiral axis is in-plane. These crystal settings enable spectroscopic measurements in the magnetochiral and transverse magnetochiral orientations, respectively [Fig. 1(c, f)]. Both are in the Faraday geometry as shown in the schematics, but the direction of applied field and light propagation are different with respect to

the chiral axis. While the magnetochiral orientation has been demonstrated in a handful of cases [3, 13, 15], the transverse magnetochiral orientation is completely unexplored - although it clearly breaks the requisite symmetries (Supplementary Information).

In this work, we demonstrate that the on-site Ni d-to-d excitations are in fact magnetoelectric in nature. Analysis of the symmetries of nonreciprocality and the spin-orbit coupling-derived features in the magneto-optical response lead to measurements of magnetochiral dichroism - in which we switch both k and H. Remarkably, these effects are in the visible part of the spectrum, broadband, and sensitive to the different spin orientations in Ni_3TeO_6. Complementary work in the transverse magnetochiral orientation reveals how constraints can be manipulated to realize distinct nonreciprocal effects in chiral materials. Further, the magnetochiral dichroism is calculated based on a first-principles methodology and compared with experimental observations. Our theoretical analysis reveals the magneoelectric nature of Ni on-site d-to-d excitations and the decisive role of atomic spin-orbit coupling in inducing the nonreciprocality. This approach promises to provide an important tool for future computational predictions of dynamic properties in a range of multiferroic materials.

RESULTS AND DISCUSSION

Nonreciprocal effects in Ni_3TeO_6

As indicated earlier, Ni_3TeO_6 has several different magnetic phases accessible under external field [Fig. 1(a)]. Except in the zero-field antiferromagnetic ground state, the symmetry conditions for the existence of nonreciprocal directional dichroism are satisfied, but one may wonder whether the effect is large enough to be detectable in the visible frequency range. Here the absorption is dominated by Ni^{2+} d-to-d on-site excitations. These are known to be magnetoelectric, not only because the excitations are sensitive to the microscopic spin arrangement in each magnetic phase [27], but also due to spin-orbit coupling, which becomes significant in the excited states.

As we shall see later, our first-principles-based theory not only estimates the d-to-d electric and magnetic dipole excitations, but also indicates that spin-orbit coupling is a critical element in the nonreciprocal directional dichroism. Specifically, the nonreciprocal component of the absorption for light propagating along the z-direction is found to be [1, 34]

$$\begin{aligned}\Delta\alpha_{\mathrm{NDD}}(\omega) &= \frac{2\omega}{c}\mathrm{Im}\left[N_+(\omega) - N_-(\omega)\right] \\ &\simeq \frac{2\omega}{c}\mathrm{Im}\left[\chi^{\mathrm{me}}_{yx}(\omega) + \chi^{\mathrm{em}}_{xy}(\omega)\right], \qquad (1)\end{aligned}$$

where $N_\pm(\omega)$ is the complex refractive index for light propagating along the $\pm z$-direction with frequency ω, and $\chi^{\mathrm{me}}_{yx}(\omega)$ and $\chi^{\mathrm{em}}_{xy}(\omega)$ are the off-diagonal components of the dimensionless magneto-electric and electromagnetic response tensors. See Eq. (2) or the Methods section for their explicit linear-response form. It will be shown in the following section that, without spin-orbit coupling, the χ^{me}_{yx} and χ^{em}_{xy} responses cancel each other, so that there is no k-direction-dependent component even in the presence of magnetism. Our first-principles calculations, presented later, suggest that a nonreciprocal directional dichroism signal on the order of one part in 10^2 should be observable for the Ni d-to-d excitations even with a relatively weak (≈30 meV) spin-orbit coupling within the Ni d shell. Hence, Ni_3TeO_6 is an outstanding candidate in which to explore nonreciprocal directional dichroism in the vicinity of d-to-d excitations in the visible range, where such effects have rarely been discussed.

With these ideas in mind, we polished two different single crystals [Fig. 1(d, g)]. Evidence for single domain character [33] - at least in the measurement area - is evident in these images, the optical rotation data [Fig. 1(e)], and elaborated in the Supplementary Information.

Figure 2 summarizes nonreciprocal directional dichroism in Ni_3TeO_6. Focusing first on the magnetochiral orientation [Fig. 2(a-f)], we find a large nonreciprocal response in the vicinity of the on-site d-to-d excitations. Changing the direction of magnetic field H while keeping k constant yields absorption difference curves ($\Delta\alpha$) that are distinct in several respects [Fig. 2(b)]. To find the nonreciprocal response, we subtract the two $\Delta\alpha$ curves: $\Delta\alpha_{\mathrm{NDD}} = \Delta\alpha_{+H} - \Delta\alpha_{-H}$ [Fig. 2(c)]. This difference corresponds to the absorption of light in one field direction versus that in the other field direction. To further test the nonreciprocal effect, we held H constant while varying the light propagation direction k [Fig. 2(d-f)]. The absorption difference spectra and $\Delta\alpha_{\mathrm{NDD}}$ are virtually identical to the data obtained by switching the direction of the applied field under constant k. Thus, in addition to revealing broad band nonrecriprocal directional dichroism at much higher energies than usual in Ni_3TeO_6, the effect is also very large. All of this work was done with unpolarized light. As a point of comparison, magnetochiral dichroism in the optical region has also been realized in CuB_2O_4 - both with and without polarized light [15]. Here, $\Delta\alpha_{\mathrm{NDD}}$ arises from the mixing of electronic- and magnetic-dipole transitions due to spin-orbit coupling which activate in turn the intra-atomic d-to-d Cu^{2+} transitions [15].

We also reached beyond the magnetochiral orientation to explore nonreciprocal directional dichroism in other settings. Our objectives are to (i) seek out strange new types of light-matter interactions in chiral magnets and (ii) to compare their character with the more established variants. Figure 1(f, g) summarizes the sample requirements (exposing the mono-chiral c-axis in the plane of the

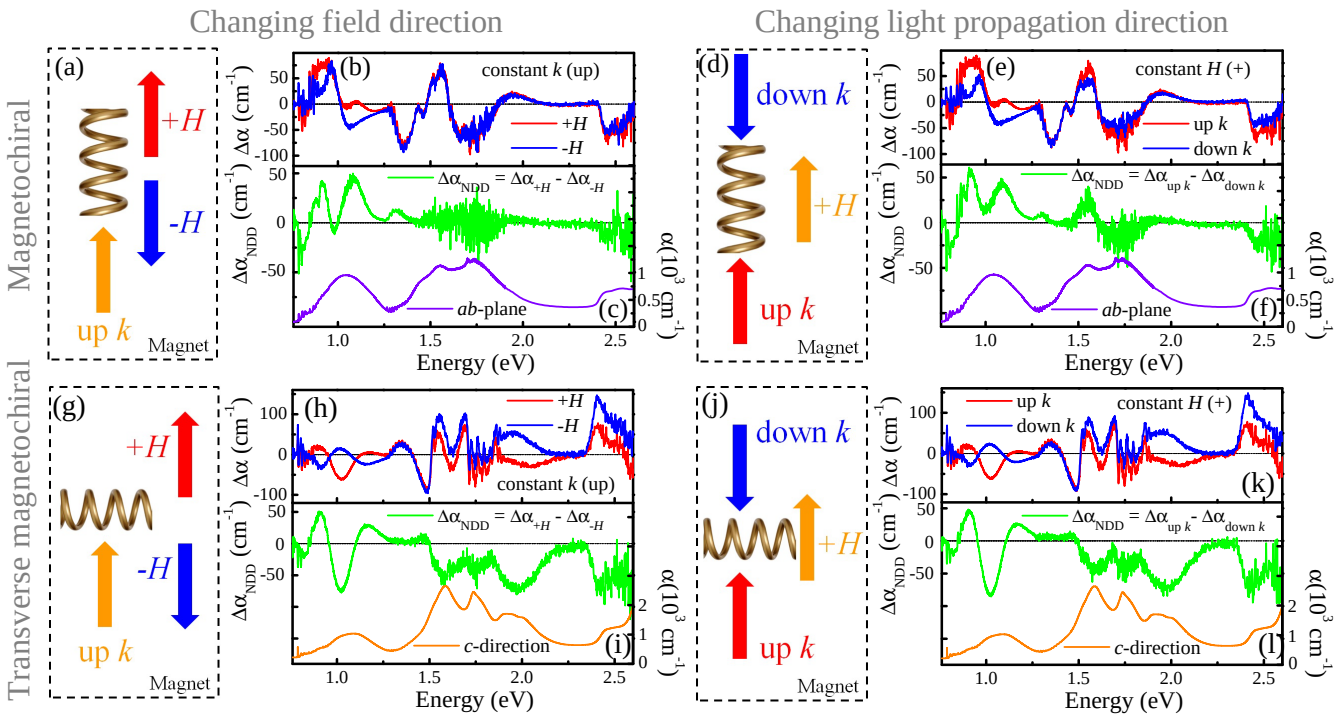

FIG. 2. **Directional dichroism for different measurement symmetries.** (a, d) Schematic view of H and k relative to the chiral axis of Ni_3TeO_6 in the magnetochiral orientation. (b) Magneto-optical response as measured by the absorption difference at full field, $\Delta\alpha = \alpha(H = \pm 62\text{ T}) - \alpha(H = 0\text{ T})$. Data in the $+H$ direction are different than those in the $-H$ direction. (c) Nonreciprocal directional dichroism of Ni_3TeO_6 in the metamagnetic phase in the magnetochiral orientation, obtained by reversing the field direction with fixed k. Thus, $\Delta\alpha_{\text{NDD}} = \alpha(H_{up} = 62\text{ T}) - \alpha(H_{down} = 62\text{ T})$ which is the same as $\Delta\alpha(H_{up} = 62\text{ T}) - \Delta\alpha(H_{down} = 62\text{ T})$. For reference in (c, f), we include the linear absorption spectrum, α. (e, f) Similar $\Delta\alpha$ and $\Delta\alpha_{\text{NDD}}$ spectra are obtained by reversing the light propagation direction under constant field. Here, $\Delta\alpha$ is $\alpha(H = +62\text{ T}) - \alpha(H = 0\text{ T})$ for $\pm k$, and $\Delta\alpha_{\text{NDD}}$ is $\alpha(k_{up}) - \alpha(k_{down})$ which is the same as $\Delta\alpha(k_{up}) - \Delta\alpha(k_{down})$ with H_{up} = 62 T. (g, j) Schematic view of H and k relative to the chiral axis of Ni_3TeO_6 in the transverse magnetochiral orientation. (h, i) Magneto-optical and nonreciprocal directional dichroism of Ni_3TeO_6 at 62 T in the transverse magnetochiral orientation obtained by reversing the field direction under constant k. For reference in (i, l) we include the linear absorption spectrum. (k, l) Similar $\Delta\alpha$ and $\Delta\alpha_{\text{NDD}}$ spectra are obtained by varying the light propagation direction under constant field.

polished single domain crystal) and Faraday measurement geometry for uncovering the nonreciprocal directional dichroism in the transverse magnetochiral orientation. The lower portion of Fig. 2 summarizes our spectroscopic results. As before, we switch both allowed parameters. We changed the applied field direction while keeping the light propagation fixed [Fig. 2(g-i)], and we varied k under constant H [Fig. 2(j-l)]. Clearly, nonreciprocal directional dichroism in the transverse magnetochiral orientation differs greatly from that in the magnetochiral orientation. Not only is $\Delta\alpha_{\text{NDD}}$ overall broader, encompassing two active spectral regimes across the near infrared and visible that are more than 0.5 eV wide, but it is also large - on the order of ± 50 cm^{-1}. More importantly, the measurement configuration is unique within the current framework of magnetochiral dichroism [3]. Again, these results were achieved with unpolarized light.

Microscopic model for nonreciprocal directional dichroims in chiral magnets

As shown in the previous literature [1, 2], nonreciprocal directional dichroism is a byproduct of magnetoelectric excitations, which in our case are the Ni^{2+} d-to-d excitations between atomic multiplet states in Ni_3TeO_6. The magnetoelectic coupling tensors $\chi^{\text{me}}_{\alpha\beta}$ and $\chi^{\text{em}}_{\alpha\beta}$ in the linear-response regime take the form [35]

$$\chi^{\text{me}}_{\alpha\beta}(\omega) = -\frac{\kappa_0}{\hbar V}\sum_n \left[\frac{M^{0n}_\alpha P^{n0}_\beta}{\omega - \omega_{n0} + i\delta} - \frac{P^{0n}_\beta M^{n0}_\alpha}{\omega + \omega_{n0} + i\delta}\right],$$
$$\chi^{\text{em}}_{\alpha\beta}(\omega) = -\frac{\kappa_0}{\hbar V}\sum_n \left[\frac{P^{0n}_\alpha M^{n0}_\beta}{\omega - \omega_{n0} + i\delta} - \frac{M^{0n}_\beta P^{n0}_\alpha}{\omega + \omega_{n0} + i\delta}\right], \quad (2)$$

where $\kappa_0 = \sqrt{\mu_0/\epsilon_0}$, $\omega_{n0} \equiv \omega_n - \omega_0$, and $M^{n0}_\alpha \equiv \langle n|M_\alpha|0\rangle$ and $P^{n0}_\beta \equiv \langle n|P_\beta|0\rangle$ are matrix elements in Cartesian directions α and β of magnetic (M) and electric (P) dipole operators respectively, taken between

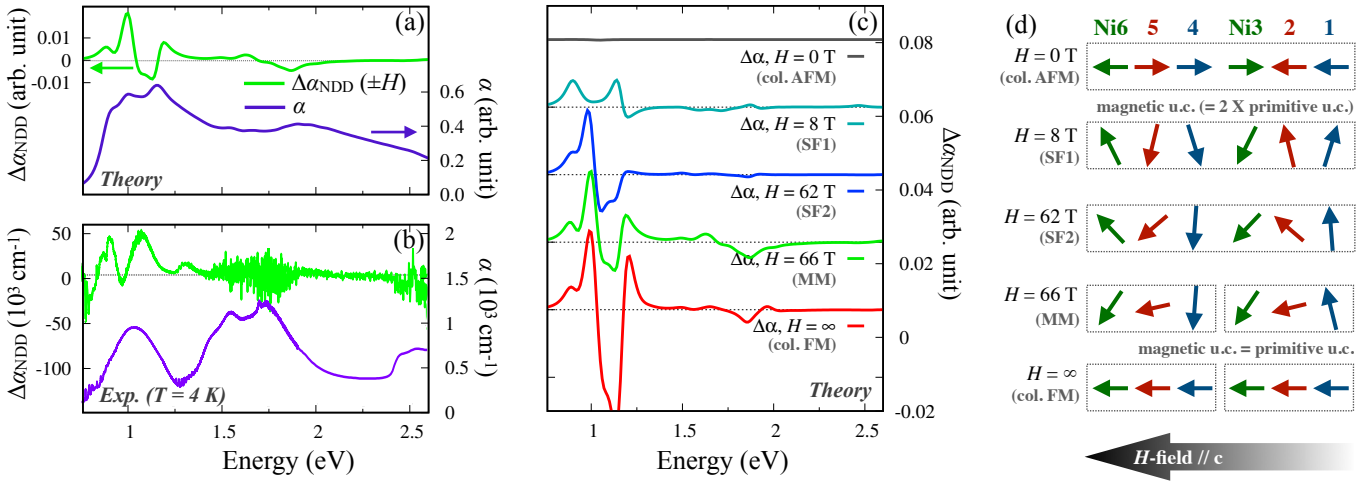

FIG. 3. **Calculated nonreciprocal optical effects.** (a) Simulated absorption spectra α and nonreciprocal responses $\Delta\alpha_{\rm NDD} \equiv \alpha(+H) - \alpha(-H)$ for the magnetic phase at $H = 66$ T from *ab-initio* calculations. (b) Experimental data in the magnetochiral configuration is shown for comparison. (c) Nonreciprocal responses from different magnetic configurations (offset vertically for clarity). (d) Spin configurations under various magnetic fields applied along c (reproduced from Ref. 26). Here SF and MM denote spin-flop and metamagnetic phases, respectively.

ground and excited ($|0\rangle$ and $|n\rangle$) d^8 atomic multiplet states respectively. The broadening δ originates from hybridizations between the Ni d shell and its environment of oxygen and other neighboring sites. Assuming the hybridization-induced broadening δ is small compared to the excitation energies ω_{n0} in the mid-gap energy range of this wide-gap ($\simeq 2.7$ eV) insulator, a calculation of $\chi^{\rm me}_{\alpha\beta}$ and $\chi^{\rm em}_{\alpha\beta}$ in an atomic-like limit can be a plausible first-order approximation. In particular, we obtain the multiplet eigenstates and dipole matrix elements from an exact diagonalization of the many-body Hamiltonian within the Ni d shell on each Ni site independently, where this Hamiltonian includes terms describing the crystal fields, exchange fields, and spin-orbit coupling as obtained from first-principles density-functional calculations [36].

The critical role of spin-orbit coupling in the nonreciprocal directional dichroism of Eq. (1) can be seen from its explicit form,

$$\Delta\alpha_{\rm NDD}(\omega) \simeq \frac{4\mu_0}{\hbar V}\omega \sum_n \frac{{\rm Re}\left[M_y^{0n} P_x^{n0}\right]\delta}{(\omega-\omega_{n0})^2+\delta^2}, \qquad (3)$$

which has been obtained by plugging Eq. (2) into (1) and keeping only the absorption part ($\omega \simeq \omega_{n0}$). When spin-orbit coupling is absent, one can choose all spatial eigenstates to be real, in which case M_y^{n0} and P_x^{0n} become purely real and imaginary, respectively, yielding ${\rm Re}\left[M_y^{0n} P_x^{n0}\right] = 0$. Hence it can be seen that the spin-orbit coupling is a critical component of the nonreciprocal effect, at least in the linear-response regime.

Figure 3 shows a summary of the calculations. Comparing Fig. 3(a) and (b), it can be seen not only that the simulation yields reasonable agreement for the ratio between the nonreciprocal and reciprocal parts of the absorption spectra, $|\Delta\alpha_{\rm NDD}/\alpha| \simeq 0.03$, but also that it reproduces the features occurring around $\omega \sim 1$ eV, which corresponds to the excitation energy from $^3{\rm A}_{2g}$ to $^3{\rm T}_{2g}$ states. Note that the vanishing of $\Delta\alpha_{\rm NDD}$ in the collinear antiferromagnetic phase is also well reproduced [35]. The agreement between theory and experiment becomes poorer near the band edge, where the itinerant character of electrons becomes more dominant.

Remarkably, the relatively small spin-orbit coupling ($\lesssim 40$ meV) gives rise to a nonreciprocal contribution up to 3% of the absorption spectra, implying even larger nonreciprocal signals may be realized in systems with stronger spin-orbit coupling. Interestingly, the weak spin-orbit coupling in Ni (about 30 meV within the t_{2g} shell) is enhanced ($30 \rightarrow 40$ meV) by the presence of Te via hybridization in this compound. This observation suggests the intriguing possibility of amplifying spin-orbit induced physics and nonreciprocal optical effects in compounds where magnetically active transition-metal atoms coexist with nonmagnetic heavy atoms in their immediate environment.

Testing the effects of switching H and k

We also sought to compare field reversal vs. light propagation effects on nonreciprocal directional dichroism in Ni_3TeO_6. Figure 4(a,b) presents $\Delta\alpha_{\rm NDD}$ under varying H and k conditions for the magnetochiral and transverse magnetochiral measurement symmetries, respectively. As anticipated for a mono-chiral system with a switchable moment, the overall shape of $\Delta\alpha_{\rm NDD}$ in Ni_3TeO_6 does not depend upon whether the magnetic

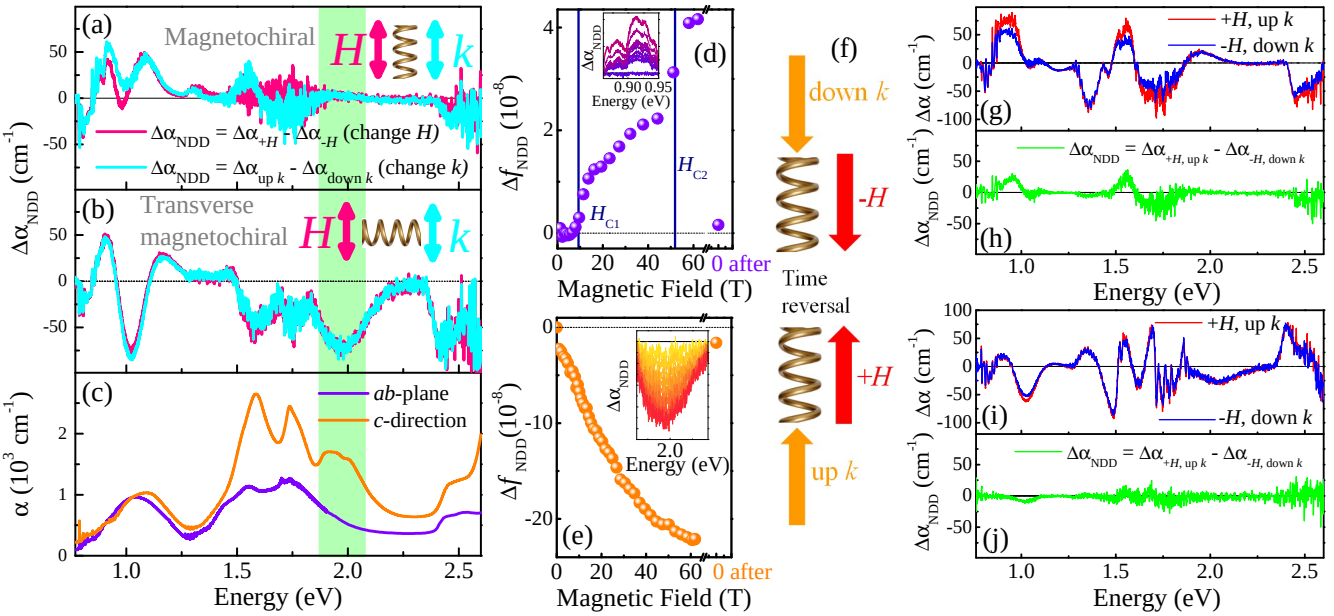

FIG. 4. **Testing the effect of switching k and H.** (a) $\Delta\alpha_{\rm NDD}$ under different field and light propagation directions in the magnetochiral orientation for Ni_3TeO_6. (b) $\Delta\alpha_{\rm NDD}$ under different field and light propagation directions in the transverse magnetochiral orientation. (c) Linear absorption spectrum at 4.2 K for reference. (d,e) Changes in the nonreciprocal response of Ni_3TeO_6, as measured by the change in oscillator strength Δf, as a of function magnetic field for the magnetochiral and transverse magnetochiral orientations, respectively. Zero field data, both before and after the field pulse, is shown. Insets display close-up views of $\Delta\alpha_{\rm NDD}$ spectra as a function of magnetic field. (f) Schematic showing the symmetry in the two scenarios when both H and k are changed. (g-j) Comparison of $\Delta\alpha$ and $\Delta\alpha_{\rm NDD}$ spectra when both H and k are switched in the magnetochiral (g,h) and transverse magnetochiral (i,j) orientations.

field or light propagation direction is switched. The response in the magneto- and transverse magnetochiral orientations is, however, quite different. In particular, $\Delta\alpha_{\rm NDD}$ in the transverse magnetochiral orientation includes a large contribution from the c-direction and, as a result, has an extra functional region (highlighted by the green band) that does not have a counterpart in the more traditional magnetochiral response. To provide additional insight into the variation of the nonreciprocal effect across the spin flop and metamagnetic transitions, we calculated the change in oscillator strength $\Delta f_{\rm NDD}$ [37] and plotted the result as a function of applied field. For the magnetochiral orientation [Fig. 4(d)], $\Delta f_{\rm NDD}$ is initially zero. This is because there is no overall magnetic moment because spins are collinear along c [26]. A small moment develops at 9 T when the spins flop into the ab-plane. Above 9 T, the spins cant with increasing field, inducing large changes in $\Delta\alpha_{\rm NDD}$. The nonreciprocal response in the transverse magnetochiral orientation is different [Fig. 4(e)]. Here, $\Delta f_{\rm NDD}$ increases gradually as the spins cant toward the field and the overall magnetic moment increases. As a reminder, the easy axis is along c and in-plane in this geometry (and perpendicular to the magnetic field). There are no hysteresis effects within our sensitivity.

From the symmetry standpoint, the nonreciprocal effect arises from the reversal of H or k [3, 38]. Further, when both H and k are switched, $\Delta\alpha_{\rm NDD}$ should vanish, as the two scenarios shown in Fig. 4(f) are related by time-reversal symmetry. We can test this supposition in Ni_3TeO_6 since we performed both sets of experiments. Figure 4(g-j) summarizes the effect of switching both field and the direction of light propagation for the two measurement orientations of interest. Turning first to the transverse magnetochiral orientation case [Fig. 4(i,j)], we find that simultaneously switching both H and k reveals almost no residual nonreciprocal response. Thus, the system is symmetric to reversal of both H and k in this configuration - as one might expect [38].

We also extracted $\Delta\alpha_{\rm NDD} = \Delta\alpha_{+H,{\rm up}k} - \Delta\alpha_{-H,{\rm down}k}$ for Ni_3TeO_6 in the magnetochiral orientation [Fig. 4(g,h)]. Here, instead, there is a small residual response indicating an apparent asymmetry in the measured nonreciprocal directional dichroism. One may wonder whether this contrast might be attributed to additional symmetry breaking due to the presence of structural chirality and/or electric polarization, but symmetry arguments indicate otherwise. That is, application of time reversal to the image in the top panel of Fig. 4(f) produces the image in the bottom panel (without reversing chirality or polarization), so the light propagation properties must be identical. To put it

another way, if one were to reverse only the polarization in the top panel, non-reciprocal directional dichroism would still be identical since the two measurements are related by a 2-fold rotation of the experimental setup about an in-plane axis followed by time reversal. (This operation reverses P but not H, k, or chirality.) We are currently uncertain about the source of the discrepancies visible in Fig. 4(g-h), but we note the polar nature of the crystal implies an inequivalence between the top and bottom crystal surfaces, and we speculate that differences in surface charge, reflectivity, roughness, adsorbed molecular species, or other properties of the surfaces could be responsible.

SUMMARY AND OUTLOOK

We bring together pulsed field techniques, optical spectroscopy, and first principles calculations to reveal the magnetoelectric character of the on-site d-to-d excitations of Ni^{2+} and their sensitivity to the spin-flop and metamagnetic transitions in Ni_3TeO_6. Analysis of the symmetry requirements for nonreciprocal directional dichroism in chiral magnets led to the discovery of this effect in both the magnetochiral and transverse magnetochiral orientations. In both cases, we find large broad band nonreciprocal effects at much higher energies than generally anticipated. These effects are up to 1.5 eV wide and ± 50 cm^{-1} in size, which is on the order of 35% at 0.79 eV. Furthermore, we test the expected equivalence of the nonreciprocal response when switching H vs. switching k. The comparison is moderately good in the magnetochiral case, and nearly exact in the transverse magnetochiral case. Our newly developed first-principles formalism enables the quantitative study of dynamical multiferroics beyond a conventional symmetry analyses, pioneering a new approach to the search for candidate functional materials. In addition, insights from our theoretical study suggest that $3d$-$4d$ or $3d$-$5d$ magnetic transition metal compounds with sizable spin-orbit coupling can be an exciting playground for optical-diode effects. Overall, our work opens the door to the exploration of chiral magnetic materials for high-energy magnetoelectric excitations, provides insight to the assumption that nonreciprocal effects are identical for varying either H or k, and presents a new orientation in which nonreciprocal effects can be studied.

METHODS

High quality single crystals were grown as described previously [25] and polished in two different orientations to thicknesses between 28 and 50 μm in order to control optical density. One orientation exposed the ab-plane whereas the other contained the c-axis in the plane of the polished surface [Fig. 1(c, f)]. Evidence for single domain character of these samples is given in Fig. 1(d, e, and g) and discussed in detail in the Supplementary Information. To reinforce our polished samples in pulsed fields, we coated them with a transparent epoxy. Optical transmittance was measured as a function of energy and temperature in the ab-plane and in the c-direction using a series of spectrometers (0.4 - 3.0 eV; 4.2 - 300 K) [27]. Absorption was calculated as $\alpha(E) = -(1/d)\ln(\mathcal{T}(E))$, where $\mathcal{T}(E)$ is the transmittance and d is the sample thickness. Magneto-optical spectroscopy was performed in the Faraday geometry at cryogenic temperatures (4.0 K) in a capacitor-driven 65 T pulsed magnet at the National High Magnetic Field Laboratory in Los Alamos, New Mexico. Our focus was on the 0.75 - 2.6 eV range with 2.4 meV resolution. Broadband light from a tungsten lamp was coupled to optical fibers and focused onto the sample for transmittance experiments. A collection fiber brought the light from the top of the probe to the grating spectrometer, where both charge-coupled device and InGaAs detectors were employed as appropriate. Spectra were taken in four different measurement configurations: ($+H$, up k), ($-H$, up k), ($+H$, down k), and ($-H$, down k). Each run was carried out sequentially and consistently, starting with one k direction (and pulsing to obtained both $\pm H$) and then switching to the other k direction (again measuring both H directions). To switch k, we swapped the optical fibers from the source to the detector and vice versa. Specific care has been taken to make sure none of the reported effects come from the optical elements in the magneto-spectroscopy setup (such as trivial Faraday rotation in the optical fibers, etc.).

First-principles density-functional theory calculations were performed using the WIEN2K full-potential code [39]; the Cerpeley-Alder LDA functional [40], $RK_{\max} = 7.0$, and a $10 \times 10 \times 10$ k-grid sampling were employed. Information on crystal fields and single-particle dipole matrix elements P_α within the Ni d-orbitals were extracted by employing orbital projectors implemented in the Embedded DMFT Functional (EDMFT) code [41]. Electric and magnetic dipole matrix elements $\mathbf{P}^{n0} \equiv \langle n|\mathbf{P}_\alpha|0\rangle$ and $\mathbf{M}^{n0} \equiv \langle n|\mathbf{M}|0\rangle$ between atomic multiplets $|0\rangle$ and $|n\rangle$ are computed with crystal fields and spin-orbit coupling incorporated via the exact diagonalization (ED) routine implemented within the EDMFT code. In practice, instead of $\mathbf{P}^{n0}$, we used matrix elements of the momentum operator $\mathbf{p}^{n0}$ to compute the response tensors; these are related by $\mathbf{P}^{n0} = \mathbf{p}^{n0}(q_e/im_e\omega_{n0})$, where q_e and m_e are the charge and mass of the electron, respectively. The OPTIC subprogram [42] in the WIEN2K package was employed to obtain the momentum matrix elements in band basis first, which were then transformed into the multiplet representation $\mathbf{p}^{n0}$ based on the knowledge of the ED eigenstates and local d-orbital projectors. Note that the same procedure was applied to obtain $\mathbf{M}^{n0} \equiv \mathbf{L}^{n0} + 2\mathbf{S}^{n0}$, where the g-factor has been set to be 2.

Four linear response tensors — electro-electric ($\chi^{\rm ee}_{\alpha\beta}$), electro-magnetic ($\chi^{\rm em}_{\alpha\beta}$), magneto-electric ($\chi^{\rm me}_{\alpha\beta}$), and magneto-magnetic ($\chi^{\rm mm}_{\alpha\beta}$) — can be computed with the quantities obtained above. These are defined according to the constitutive relations for the **D** and **B** fields,

$$\begin{aligned}\mathbf{D} &= \epsilon_0(1+\chi^{\rm ee})\mathbf{E} + \sqrt{\epsilon_0\mu_0}\chi^{\rm em}\mathbf{H},\\ \mathbf{B} &= \mu_0(1+\chi^{\rm mm})\mathbf{H} + \sqrt{\epsilon_0\mu_0}\chi^{\rm me}\mathbf{E}.\end{aligned} \tag{4}$$

Explicit forms for the magnetoelectric response tensors χ^{me} and χ^{em} were already given in Eq. (2), and the corresponding expressions for the electric and magnetic susceptibilities, which were used to compute the absorption spectra, are

$$\begin{aligned}\chi^{ee}_{\alpha\beta}(\omega) &= -\frac{1}{\hbar V\epsilon_0}\sum_n\left[\frac{P^{0n}_\alpha P^{n0}_\beta}{\omega-\omega_{n0}+i\delta} - \frac{P^{0n}_\beta P^{n0}_\alpha}{\omega+\omega_{n0}+i\delta}\right],\\ \chi^{mm}_{\alpha\beta}(\omega) &= -\frac{\mu_0}{\hbar V}\sum_n\left[\frac{M^{0n}_\alpha M^{n0}_\beta}{\omega-\omega_{n0}+i\delta} - \frac{M^{0n}_\beta M^{n0}_\alpha}{\omega+\omega_{n0}+i\delta}\right].\end{aligned} \tag{5}$$

Then the refractive index for light propagating along $z \parallel \mathbf{c}$ can be calculated as [1, 34, 35],

$$\begin{aligned}N_{s_k}(\omega) \equiv& N_0(\omega) + \Delta N_{s_k}(\omega)\\ \simeq& \sqrt{\left[1+\chi^{\rm ee}_{xx}(\omega)\right]\left[1+\chi^{\rm mm}_{yy}(\omega)\right]}\\ &+ s_k\,\frac{\chi^{\rm me}_{yx}(\omega)+\chi^{\rm em}_{xy}(\omega)}{2},\end{aligned} \tag{6}$$

where s_k is the sign of the k-vector. Plugging this expression for the refractive index into the first line of Eq. (1) yields the second line of Eq. (1) in the manuscript.

The strength of the spin-orbit coupling within the Ni d shell was estimated via a Wannierization routine [43, 44] implemented in the OPENMX code [45]. The estimated size of the spin-orbit coupling within the Ni t_{2g} shell was about 42 meV. The contribution from Te was estimated to be about 10 meV from a separate estimation of the spin-orbit coupling in Ni_3SO_6 (assuming the spin-orbit coupling from sulfur is almost negligible). Magnetic orders were incorporated in the form of effective exchange fields exerted upon each site originating from the surrounding magnetic background. The directions of the effective exchange fields, e.g., the directions of the Ni magnetic moments in each magnetic configuration under the external field, were employed from Ref. 26. The size of the exchange field was chosen to be 50 meV, and the results do not visibly depend on this size once the splitting of the ground states becomes larger than the thermal energy scale ($T \lesssim 10$K in this work). Details of the computational methods will be published elsewhere [46].

ACKNOWLEDGEMENTS

Research at the University of Tennessee and Rutgers University is supported by the NSF-DMREF program (DMR-1629079 and DMR-1629059). A portion of this research was performed at the National High Magnetic Field Laboratory which is supported by the National Science Foundation DMR-1644779, the State of Florida, and the U.S. Department of Energy.

AUTHOR CONTRIBUTIONS

M.O.Y. and J.L.M. designed the study. J.Y. and S.W.C. grew the crystals, M.O.Y. polished the samples, and J.W.K. and S.W.C. confirmed the mono-chiral domain character of the polished crystals. M.O.Y., J.L.M., and S.W.C. discussed the measurement configurations and run pattern in detail. M.O.Y., K.D.H., K.R.O., S.C., A.V.S., and J.L.M. performed the pulsed field optical measurements, and M.O.Y. and J.L.M. analyzed the spectral data. H.S.K., K.H., and D.V. developed a microscopic model for nonreciprocal optical effects and applied it to Ni_3TeO_6. M.O.Y., H.S.K., K.H., D.V., and J.L.M. wrote the manuscript. All authors commented on the final version of the text.

REFERENCES

[1] Kézsmárki, I., *et al.* One-way transparency of four-coloured spin-wave excitations in multiferroic materials. *Nat. Commun.* **5**, 3203 (2014).

[2] Tokura, Y. & Nagaosa, N. Nonreciprocal responses from non-centrosymmetric quantum materials. *Nat. Commun.* **9**, 3740 (2018).

[3] Cheong, S.-W., Talbayev, D., Kiryukhin, V., & Saxena, A. Broken symmetries, non-reciprocity, and multiferroicity. *npj Quantum Mater.* **1**9, 1 (2018).

[4] Qin, F., *et al.* Superconductivity in a chiral nanotube. *Nat. Commun.* **8**, 14465 (2017).

[5] Aoki, R., Kousaka, Y., & Togawa Y. Anomalous nonreciprocal electrical transport on chiral magnetic order. *Phys. Rev. Lett.* **1**22, 057206 (2019).

[6] Kwon, J. H. Giant nonreciprocal emission of spin waves in Ta/Py bilayers. *Sci. Adv.* **2**, 1501892 (2016).

[7] Stock, C., *et al.* Magnon directional anisotropy under broken time reversal symmetry in antiferromagnetic $Ba_3NbFe_3Si_2O_14$. under review at *Phys. Rev. Lett.* (2019).

[8] Kravchuk, V. P., Röbler, U. K., van den Brink, J., & Garst, M. Solitary wave excitations of skyrmion strings in chiral magnets. *a*rXiv:1902.01420v1 (2019).

[9] Szaller, D., Bordács, S., & Kézsmárki, I. Symmetry conditions for nonreciprocal light propagation in magnetic crystals. *Phys. Rev. B* **87**, 014421 (2013).

[10] Kézsmárki, I., *et al*. Enhanced directional dichroism of terahertz light in resonance with magnetic excitations of the multiferroic $Ba_2CoGe_2O_7$ oxide compound. *Phys. Rev. Lett.* **1**06, 057403 (2011).

[11] Bordács, S., *et al*. Unidirectional terahertz light absorption in the pyroelectric ferrimagnet $CaBaCo_4O_7$. *Phys. Rev. B* **9**2, 214441 (2015).

[12] Rikken, G. L. J. A., Strohm, C., & Wyder, P. Observation of magnetoelectric directional anisotropy. *Phys. Rev. Lett.* **8**9, 13 (2002).

[13] Bordács, S., *et al*. Chirality of matter shows up via spin excitations. *Nat. Phys.* **8**, 734 (2012).

[14] Saito, M., Taniguchi, K., & Arima, T.-h. Gigantic optical magnetoelectric effect in CuB_2O_4. *J. Phys. Soc. Jpn.* **7**7, 013705 (2008).

[15] Saito, M., Ishikawa, K., Taniguchi, K., & Arima, T. Magnetic control of crystal chirality and the existence of a large magneto-optical dichroism effect in CuB_2O_4. *Phys. Rev. Lett.* **1**01, 117402 (2008).

[16] Rikken, G. L. J. A. & Raupach, E. Observation of magneto-chiral dichroism. *Nature* **3**90, 493 (1997).

[17] Sessoli, R., *et al*. Strong magneto-chiral dichroism in a paramagnetic molecular helix observed by hard X-rays. *Nat. Phys.* **1**1, 69 (2015).

[18] Nakagawa, N., *et al*. Magneto-chiral dichroism of $CsCuCl_3$. *Phys. Rev. B* **9**6, 121102(R) (2017).

[19] Train, C., Gruselle, M., & Verdaguer, M. The fruitful introduction of chirality and control of absolute configurations in molecular magnets. *Chem. Soc. Rev.* **4**0, 3297 (2011).

[20] Barron, L. D. Chirality and magnetism shake hands. *Nat. Mater.* **7**, 691 (2008).

[21] Train, C., *et al*. Strong magneto-chiral dichroism in enantiopure chiral ferromagnets. *Nat. Mater.* **7**, 729 (2008).

[22] Yu, S., *et al*. High-temperature terahertz optical diode effect without magnetic order in polar $FeZnMo_3O_8$. *Phys. Rev. Lett.* **1**20, 037601 (2018).

[23] Kézsmárki, I., *et al*. Optical diode effect at spin-wave excitations of the room-temperature multiferroic $BiFeO_3$. *Phys. Rev. Lett.* **1**15, 127203 (2015).

[24] Lee, J. H., Kézsmárki, I., & Fishman, R. S. First-principles approach to the dynamic magnetoelectric couplings for the non-reciprocal directional dichroism in $BiFeO_3$. *New J. Phys.* **1**8, 043025 (2016).

[25] Oh, Y. S., *et al*. Non-hysteretic colossal magnetoelectricity in a collinear antiferromagnet. *Nat. Commun.* **5**, 3201 (2014).

[26] Kim, J. W., *et al*. Successive magnetic-field-induced transitions and colossal magnetoelectric effect in Ni_3TeO_6. *Phys. Rev. Lett.* **1**15, 137201 (2015).

[27] Yokosuk, M. O., *et al*. Magnetoelectric coupling through the spin flop transition in Ni_3TeO_6. *Phys. Rev. Lett.* **1**17, 147402 (2016).

[28] Jung, J. H., *et al*. Optical magnetoelectric effect in the polar $GaFeO_3$ ferrimagnet. *Phys. Rev. Lett.* **9**3, 037403 (2004).

[29] Toyoda, S., *et al*. One-way transparency of light in multiferroic CuB_2O_4. *Phys. Rev. B* **1**15, 267207 (2015).

[30] Saito, M., Ishikawa, K., Taniguchi, K., & Arima, T.-h. Magnetically controllable CuB_2O_4 phase retarder. *Appl. Phys. Express* **1**, 121302 (2008).

[31] Saito, M., Ishikawa, K., Konno, S., Taniguchi, K., & Arima, T. Periodic rotation of magnetization in a non-centrosymmetric soft magnet induced by an electric field. *Nat. Mater.* **8**, 634 (2009).

[32] Živković, I., Prša, K., Zaharki, O., & Berger, H. Ni_3TeO_6 - a collinear antiferromagnet with ferromagnetic honeycomb planes. *J. Phys. Condens. Matter* **2**2, 056002 (2010).

[33] Wang, X., Huang, F.-T., Yang, J., Oh, Y. S., & Cheong, S.-W. Interlocked chiral/polar domain walls and large optical rotation in Ni_3TeO_6. *APL Mater.* **3**, 076105 (2015).

[34] Miyahara, S., & Furukawa, N. Nonreciprocal directional dichroism and toroidalmagnons in helical magnets. *J. Phys. Soc. Jpn.* **8**1, 023712 (2012).

[35] Muthukumar, V. N., Valent, R., & Gros, C. Theory of nonreciprocal optical effects in antiferromagnets: The case of Cr_2O_3. *Phys. Rev. B* **5**4, 433 (1996).

[36] We employed WIEN2K [39], OPENMX [45], and the Embedded DMFT Functional codes [41] to compute the crystal fields, atomic multiplet levels, and the dipole matrix elements. Please refer to the Methods section for computational details.

[37] For the oscillator strength analysis, $\Delta f_{\mathrm{NDD}} = (2c)/(N_e \pi \omega_p^2) \int_{E_1}^{E_2} n \Delta\alpha_{\mathrm{NDD}}(E) dE$, where N_e is the number of electrons per Ni site, n is the refractive index, ω_p is the plasma frequency $\omega_p \equiv \sqrt{(e^2\rho)/(m\epsilon_0)}$, e and m are the charge and mass of an electron, ϵ_0 is the vacuum dielectric constant, ρ is the density of Ni sites, c is the speed of light, and E_1 and E_2 are the energy limits of integration.

[38] Hlinka, J. Eight types of symmetrically distinct vectorlike physical quantities. *Phys. Rev. Lett.* **1**13, 165502 (2014).

[39] Blaha, P., Schwarz, K., Madsen, G. K. H., Kvasnicka, D., & Luitz, J. *W*IEN2k, An augmented plane wave + local orbitals program for calculating crystal properties. Karlheinz Schwarz, Techn. Universität Wien, Austria (2001).

[40] Ceperley, D. M. and Alder, B. J. Ground state of the electron gas by a stochastic method. *Phys. Rev. Lett.* **4**5, 566 (1980).

[41] Haule, K. Structural predictions for correlated electron materials using the functional dynamical mean field theory approach. *J. Phys. Soc. Jpn.* **8**7, 041005 (2018).

[42] Ambrosch-Draxl, C., & Sofo, J. O. Linear optical properties of solids within the full-potential linearized augmented planewave method. *Comp. Phys. Commun.* **1**75, 1 (2006).

[43] Marzari, N., Mostofi, A. A., Yates, J. R., Souza, I., & Vanderbilt, D. Maximally localized Wannier functions: Theory and applications. *Rev. Mod. Phys.* **8**4, 1419 (2012).

[44] Weng, H., Ozaki, T., & Terakura, K. Revisiting magnetic coupling in transition-metal-benzene complexes with maximally localized Wannier functions. *Phys. Rev. B* **7**9, 235118 (2009).

[45] Ozaki, T. Variationally optimized atomic orbitals for large-scale electronic structures. *Phys. Rev. B* **6**7, 155108 (2003).

[46] Kim, H.-S., Yokosuk, M. O., Musfeldt, J. L., Haule, K., & Vanderbilt, D., unpublished.